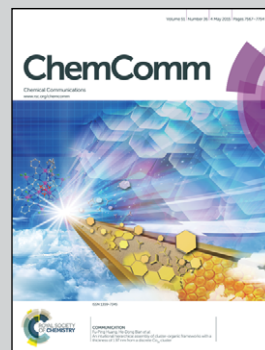


Showcasing work from Ekaterina Skorb's laboratories at the Max Planck Institute of Colloids and Interfaces, Germany, the Belarusian State University, Belarus, and the University of Bayreuth, Germany

Sonogenerated metal-hydrogen sponges for reactive hard templating

Sonochemically generated microbubbles can be considered as microreactors containing free radicals and excited species. The unique conditions of such "Bubbles HARD ROCK" can be effectively used for chemical synthesis and nanostructuring of solids.

### As featured in:



See Ekaterina V. Skorb et al.,  
*Chem. Commun.*, 2015, **51**, 7606.



Cite this: *Chem. Commun.*, 2015, 51, 7606

Received 16th December 2014,  
Accepted 12th February 2015

DOI: 10.1039/c4cc10026c

www.rsc.org/chemcomm

## Sonogenerated metal-hydrogen sponges for reactive hard templating†

Olga Baidukova,<sup>a</sup> Helmuth Möhwald,<sup>a</sup> Aliaksei S. Mazheika,<sup>b</sup> Dmitry V. Sviridov,<sup>b</sup> Tatiana Palamarcuic,<sup>c</sup> Birgit Weber,<sup>c</sup> Pavel V. Cherepanov,<sup>d</sup> Daria V. Andreeva<sup>d</sup> and Ekaterina V. Skorb<sup>\*ab</sup>

**We present sonogenerated magnesium-hydrogen sponges for effective reactive hard templating. Formation of differently organized nanomaterials is possible by variation of sonochemical parameters and solution composition: Fe<sub>2</sub>O<sub>3</sub> nanorods or composite dendritic Fe<sub>2</sub>O<sub>3</sub>/Fe<sub>3</sub>O<sub>4</sub> nanostructures.**

Synthesis of nanostructured materials by using a reactive hard template (RHT) approach was first introduced in 2007 by Thomas *et al.*<sup>1</sup> with great advantage of omitting high temperatures or harsh reagents for removal of a template. Herein we combine both RHT and the sonochemical approaches to synthesise hierarchically structured materials and propose a novel method of template-assisted synthesis of nanostructures by using sonochemistry (sono-RHT, Fig. 1). The sono-RHT concept, which combines the advantages of hard templating with *in situ* decomposition, *i.e.*, removal of a template, is a time saving and step-reducing process.

Synthesis and nanostructuring of solids by using sonochemical methods attract fundamental and technological interest due to the unique potential of locally generated high temperature (up to 5000 K) and high pressure (several hundreds of bars) processes provided by intensive ultrasonication.<sup>2a</sup> The propagation of the acoustic waves in liquid generates a cavitation field consisting of a large number of interacting microbubbles.<sup>2b</sup> These microbubbles can be considered as microreactors containing free radicals and excited species that can be used for chemical synthesis and nanostructuring of solids.<sup>2c</sup> Symmetric and asymmetric microbubble collapses can provide constant delivery of chemicals to the reaction zone.<sup>2d</sup> Recently, we demonstrated that inorganic materials could adopt a variety of different morphologies upon sonication of aqueous suspensions of solid particles. For instance,

depending on sonication time, amorphous or crystalline silicon particles and quantum dots can be formed from silicon slurries.<sup>3a</sup> Sonochemical modification of Zn particles<sup>3b</sup> leads to the formation of nanocomposite particles where ZnO nanorods are attached to the metallic Zn core. Sonochemically modified Al and Mg<sup>3c</sup> exhibit a mesoporous inner structure and a significantly increased surface area (up to 300 m<sup>2</sup> g<sup>-1</sup>). The mechanism of ultrasound-assisted modification of solid particles in water relies on the interplay of the sonomechanical effect – fragmentation of particles accompanied by the increase of the surface area and the sonochemical effect – the interfacial Red/Ox reactions and etching of a metal surface triggered by free radicals formed during water sonolysis. The contribution of these two sono-effects depends on physical (melting point, hardness, and crystallinity) and chemical (electrode potentials) properties of the metals. Furthermore, the sonochemical

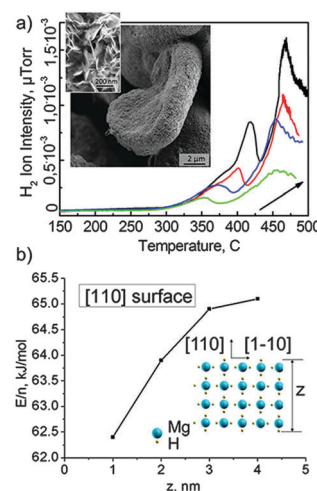


**Fig. 1** (a) Temperature programmed desorption of hydrogen from the sonogenerated metal-hydrogen sponge for reactive hard templating (sono-RHT); arrows show a ramping rate increase from 5 K min<sup>-1</sup> to 20 K min<sup>-1</sup> with the 5 K min<sup>-1</sup> step. Insets show SEM and TEM images of sono-RHT. (b) Normalized per number of Mg-atoms desorption energies of hydrogen of different thickness slabs within the DFT level.

<sup>a</sup> Max Planck Institute of Colloids and Interfaces, Am Mühlenberg 1, 14424 Potsdam, Germany. E-mail: skorb@mpikg.mpg.de

<sup>b</sup> Belarusian State University, 220030 Minsk, Belarus

<sup>c</sup> Inorganic Chemistry II, University of Bayreuth, Germany

<sup>d</sup> Physical Chemistry II, University of Bayreuth, Germany

† Electronic supplementary information (ESI) available. See DOI: 10.1039/c4cc10026c



oxidation of “reactive” metals (Al and Mg) is followed by the production of a highly concentrated reducing agent, *e.g.* hydrogen, on the metal surface.

The “reactive” Al and Mg are not only oxidized during ultrasonic treatment in water, but they also serve as effective donors of electrons that result in  $H_2$  production. Sonochemical modification of Al and Mg leads to the simultaneous formation of mesoporous metal frameworks and generation of  $H_2$  in the pores. Magnesium as one of the most reactive metals was used as a model reactive metal for the proof of the principles of sono-RHT. The images of Mg used as a sono-RHT are shown in Fig. 1a(insets). Sonication of aqueous suspensions of Mg leads to the formation of highly active magnesium hydrides of different compositions. The temperature programmed desorption of hydrogen (Fig. 1a) indicates the presence of hydrogen in the sonicated Mg. Moreover several adsorbed hydrogen clusters can be suggested since there are at least two peaks visible in the spectrum.

The calculated energy of hydrogen desorption is *ca.* 65.7 kJ and *ca.* 389.3 kJ. The magnesium hydrides rapidly decompose under extreme conditions during sonication in water with the production of  $H_2$ , and thus, magnesium is a promising material that can be used for the sono-RHT synthesis. The concentration of the residual hydrogen in the sonicated and dried Mg powder was calculated *ca.*  $1.13 \mu\text{L mg}^{-1}$ .

Both Mg and  $MgH_x$  clusters can be formed. Some of the possible geometries of  $MgH_x$  were calculated recently by the density functional theory (DFT) (B97) method.<sup>4a</sup> Comparable to our sono-RHT are hydrogen-enriched  $Mg_{15}H_x$  clusters, which were also taken into account. The extra hydrogen atoms are less strongly bound to the hydride structure and can therefore be released at lower temperatures. Moreover in our case we formed mesoporous sponge structures in which clusters are difficult to be aggregated. Mesoporous sponge has different nanosized units of  $MgH_x$  slabs in the composition. We calculated for different thickness for  $MgH_2$  crystal (100) slabs the energy of total hydrogen desorption from each single slab by DFT within the hybrid PBE0 method.<sup>4b</sup> It was shown that complimentary to our experimental data are slabs with thickness between 2 and 3 nm. The entire dehydrogenation of  $MgH_2$  slabs, the sum of desorption energies of all H-layers, is about  $65 \text{ kJ mol}^{-1}$  for (110) with  $z = 3 \text{ nm}$  (Fig. 1b). This value is very close to the experimentally obtained value. The  $\Delta H_{298}^0$  of entire dehydrogenation was calculated only for the 1 nm slab (110) due to the high computational effort needed. It is  $59.3 \text{ kJ mol}^{-1}$ , whereas electronic energy is  $62.3 \text{ kJ mol}^{-1}$ . The difference of  $3 \text{ kJ mol}^{-1}$  is vanishingly small, less than the error of application of different exchange–correlation functionals. In such a way, the first peak of  $H_2$  thermodesorption ( $65.7 \text{ kJ mol}^{-1}$ ) is most probably the desorption of the whole hydrogen from  $MgH_2$  nanoparticles of several nm size. This is less than  $\Delta_f H_{298}^0$  ( $MgH_2$ )  $-76.46 \text{ kJ mol}^{-1}$  due to the unique morphology of  $MgH_x$  used for sono-RHT and is promising fact for solid hydrogen storage.

Overall a general sono-RHT synthetic procedure of nanostructures includes the following steps: (i) sonochemical formation of the mesoporous metal RHT; (ii) ultrasound assisted loading

of the RHT with chemical precursors for nanoparticle synthesis; (iii) reduction of precursors due to interaction with the sono-activated metal surface; and (iv) the RHT decomposition due to the electrochemical processes stimulated by ultrasound. Herein, we demonstrate the sono-RHT for the synthesis of hierarchically structured materials.

Magnetic nanoparticles were synthesized by reduction of Fe(II) or Fe(III) ions from the corresponding chloride (Fig. 2) or nitrate (not shown here) salts. The formation of the magnetic iron-based materials in the pores of the sono-RHT (Mg) was followed by simultaneous electrochemical degradation of the RHT triggered by sonication. The morphology and composition of magnetic nanoparticles are dependent on the used precursors. The final magnetic materials are dark brownish powders that are composed of 4/m 3 2/m  $Fe_3O_4 - 32/m Fe_2O_3$  (Fig. S2 right and Table S1, ESI†) or 32/m  $Fe_2O_3$  (Fig. S2 left and Table S1, ESI†). By using the sono-RHT method it is possible to control the parameters during the synthesis such as concentration of the RHT, concentration and type of precursors and solvent as well as duration and intensity of sonication, *etc.* Certain equilibrium structures can be obtained under particular preparation conditions.

The sono-RHT synthesis was performed by sonication of 1 wt% aqueous suspension of *ca.* 100  $\mu\text{m}$  magnesium particles. Then aqueous solutions of iron salts (to achieve a concentration of 2 wt% in the resultant solution) were added to the suspension. The structures in Fig. S2 left (ESI†) correspond to the samples that are prepared by using a  $FeCl_2$  precursor. The structures in

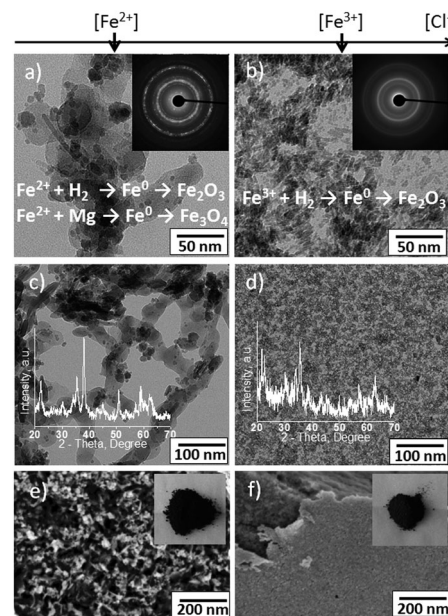


Fig. 2 Characterisation of magnetic materials formed by the sono-RHT method. (a–d) TEM images of (a, c)  $Fe_3O_4$ – $Fe_2O_3$  dendritic structure, insets show (a) electron diffraction (ED) of the sample, both hydrogen and magnesium are introduced as reduction agents with  $Fe^0$  as the intermediate, (c) XRD pattern. (b, d)  $Fe_2O_3$  magnetic rod-shaped nanoparticles, insets show (b) ED of the sample and point hydrogen as the main reduction agent with  $Fe^0$  as the intermediate, (d) XRD pattern; (e, f) SEM images of (e) dendritic structures and (f) nanoparticles; insets show optical images of the samples.





Fig. S2 right (ESI†) correspond to the samples that are synthesized in the presence of a  $\text{FeCl}_3$  precursor.

By using the same concentration of the iron salts,  $\text{Cl}^-$  concentration was higher in the presence of  $\text{FeCl}_3$ . Since the  $\text{Cl}^-$  anions are known as corrosive agents for Mg we expect that the degradation of the metal sono-RHT will be faster at higher chloride concentrations. Indeed, the degradation of Mg was slower in the presence of nitrate and  $\text{FeCl}_2$  in comparison to the degradation of the RHT in the presence of  $\text{FeCl}_3$ . The rate of Mg degradation strongly affects the morphology and composition of the resultant iron-based materials. In the case of slow decomposition of the sono-RHT decomposition process,  $\text{Mg}^0$  from the metal framework could be involved in the reduction process together with hydrogen as an additional reduction agent. This results in the formation of the iron-based dendritic porous structure on the surface of the metal surface as evidenced by TEM images (Fig. S2 left, ESI†). Since the sonication was performed in aqueous media, reduced iron nanostructures are rapidly oxidized with the formation of various iron oxides. Thus, a hierarchically structured iron based material consisting of a dendritic porous substance covered by nanoparticles was formed by using the sono-RHT method. The chemical composition of these structures will be discussed below. Shortly, the dendritic porous  $\text{Fe}_3\text{O}_4\text{-Fe}_2\text{O}_3$  is covered by  $\text{Fe}_2\text{O}_3$  nanoparticles.

If the reduction agent is mostly  $\text{H}_2$ , which is produced during the course of the fast decomposition of the magnesium framework (at high  $\text{Cl}^-$  concentration when  $\text{FeCl}_3$  is used), rod-shaped  $\text{Fe}_2\text{O}_3$  nanoparticles are formed (Fig. S2 right, ESI†).

The results of the magnetization measurements of the iron based nanoparticles and dendritic structures are shown in Fig. 3. All samples show a superparamagnetic behaviour. The material itself is ferromagnetic, thus the observed magnetic moment is much higher than for paramagnets and the sample does not follow the Curie law. However, there is no hysteresis because the particles are small: they change their orientation when the orientation of the external magnetic field is changed. This is observed when the particle size is smaller than the size of the Weiss areas of the ferromagnet/ferrimagnet. The temperature dependence was investigated in order to see, if the movement of the particles is blocked below a certain temperature (blocking temperature), which is not the case.

The Mössbauer spectrum (Fig. 3a) of the dendritic particles (Fig. S2 left, ESI†) can be approximated by a superposition of two doublets and two sextets (Table S1, ESI†). The values of quadrupole splitting (QS) to input  $A$  of the doublet of the outer shell and core  $\text{Fe}^{3+}$  decrease in comparison with the values measured for the nanoparticles mostly due to the size effect. (Fig. S2 left, ESI†). It is seen from Fig. 3a that in the case of the dendritic structure there is one maximum in total QS distribution due to an increase in the range of distributions of QS of each doublet, with a decrease of the value of the quadrupole splitting of iron ions from the outer shell of the nanoparticles. The spectrum and distribution of QS for the dendritic structures suggested their porous character which is also seen from electron microscopy (Fig. S2 left, ESI†). The presence of two sextets indicates a magnetic interaction between iron atoms in the dendritic structure. The parameters (Table S1, ESI†) of the

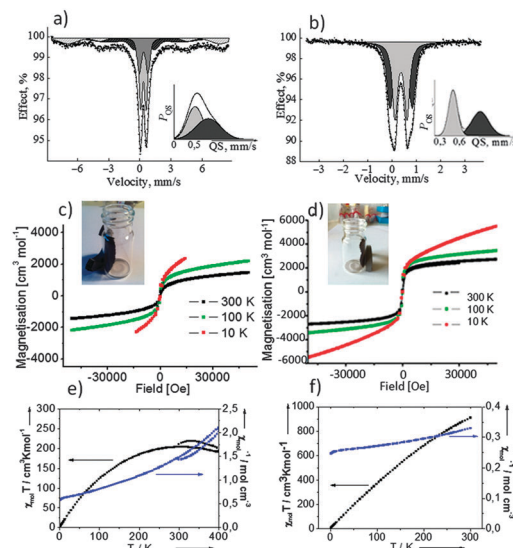


Fig. 3 Magnetic properties and structure analysis. (a, b) Mössbauer spectra (MS) of (a) dendritic particles and (b) nanoparticles. (c, d) Magnetisation at different temperatures of (c) dendritic particles and (d) nanoparticles; insets show optical images of dried powder attraction and orientation by a constant magnet in glass tubes. (e, f)  $\chi_{\text{mol}}$  and  $\chi_{\text{mol}}/T$  vs.  $T$  plots of (e) dendritic and (f) nanoparticles in the temperature range 300–0 K.

sextets (IS) might be assigned to ferromagnetic magnetite  $\text{Fe}_3\text{O}_4$ .<sup>5a</sup> One of the sextets with parameters  $\text{IS} = 0.28 \pm 0.01 \text{ mm s}^{-1}$  and  $H_{\text{eff}} = 48.0 \pm 0.02 \text{ T}$  corresponds to  $\text{Fe}^{3+}$  ions, which are in tetrahedral positions ( $A$ -position). Simultaneously the second sextet with parameters  $\text{IS} = 0.51 \pm 0.01 \text{ mm s}^{-1}$  and  $H_{\text{eff}} = 44.4 \pm 0.02 \text{ T}$  corresponds to  $\text{Fe}^{2,5+}$  ions (mixture of  $\text{Fe}^{3+}$  and  $\text{Fe}^{2+}$ ), which are in an octahedron coordination ( $B$ -positions) in spinel magnetite. The stoichiometric ratio of the first to the second sextets is close to the theoretical value of 2 ( $A_{\text{B}}/A_{\text{A}} \sim 2.1$ ).

The Mössbauer spectrum (Fig. 3b) of the nanoparticles (Fig. S2 right, ESI†) is a superposition of two doublets with approximately the same values of the isomeric shift ( $\text{IS} = 0.38 \pm 0.02 \text{ mm s}^{-1}$ ), corresponding to iron(III) ions, and different values of quadrupole splitting ( $\text{QS} = 0.50 \pm 0.02 \text{ mm s}^{-1}$  and  $\text{QS} = 0.91 \pm 0.02 \text{ mm s}^{-1}$ ). The parameters can be attributed to  $\text{Fe}_2\text{O}_3$  in the superparamagnetic state.<sup>5b</sup> Thus, intermediate  $\text{Fe}^0$  is not observed in the structure of the nanoparticles. However, the quadrupole splitting suggests the asymmetric density of the electric charge from iron ions in the core ( $\text{QS} = 0.91 \text{ mm s}^{-1}$ ) to the outer shell ( $\text{QS} = 0.50 \text{ mm s}^{-1}$ ) of the particle and justifies the assumption of an intermediate.

In order to compare the proposed sono-RHT method with a conventional method of synthesis of iron based materials we performed the synthesis with and without sonochemical irradiation of a solution of the Mg RHT and the iron(III) salt. Two types of particles and their magnetic behaviour are shown in Fig. S1 (ESI†). It is seen that particles prepared using a sono-RHT and described in the paper are different from non-magnetic particles prepared when a Mg RHT was not sonochemically irradiated.



In summary, the combination of the sonochemical approach and the RHT concept for a sono-RHT opens great prospects for the formation of a variety of nanomaterials in aqueous solutions. The structures that can be obtained are affected by the preparation conditions. The acoustic cavitation in water and the shape-defining effect of the reactive template material provide the special thermodynamic and kinetic conditions for the synthesis of nanostructures of particular morphology. The results presented here provide guidelines for the expansion of the concept towards a broad variety of chemical systems. As one of the following perspectives of the method we would like to highlight the formation of biocompatible nanostructures. Thus the hybrid inorganic–organic biocompatible structures with polypyrrole<sup>6</sup> can find their application in biosensors, bioactuators, and even nanorobotics.

The present research was supported by SFB840 (TP A10, A11). D.V.S. acknowledges the support from the Basic Research Foundation of Belarus under the grant # X13-054.

## Notes and references

- 1 A. Fischer, M. Antonietti and A. Thomas, *Adv. Mater.*, 2007, **19**, 264.
- 2 (a) K. S. Suslick, L. A. Crum and L. A. Enycl, *Acoustics*, Wiley-Interscience, N.Y., 1997; (b) L. H. Thompson and L. K. Doraiswamy, *Ind. Eng. Chem. Res.*, 1999, **38**, 1215; (c) D. G. Shchukin, E. V. Skorb, V. Belova and H. Möhwald, *Adv. Mater.*, 2011, **23**, 1922; (d) D. G. Shchukin and H. Möhwald, *Phys. Chem. Chem. Phys.*, 2006, **8**, 3496.
- 3 (a) E. V. Skorb, D. V. Andreeva and H. Möhwald, *Angew. Chem. Int. Ed.*, 2012, **51**, 5138; (b) J. Dulle, S. Nemeth, E. V. Skorb and D. V. Andreeva, *RCS Advances*, 2012, **2**, 12460; (c) E. V. Skorb, D. Fix, D. G. Shchukin, H. Möhwald, D. V. Sviridov, R. Mousa, N. Wanderka, J. Schöferhans, N. Pazos-Perez, A. Fery and D. V. Andreeva, *Nanoscale*, 2011, **3**, 985.
- 4 (a) R. W. P. Wagemans, J. H. Lenthe, P. E. Jongh, A. J. Dillen and K. P. Jong, *J. Am. Chem. Soc.*, 2005, **127**, 16675; (b) C. Adamo and V. Barone, *J. Chem. Phys.*, 1999, **110**, 6158.
- 5 (a) G. F. Goya, T. S. Berquo, F. C. Fonseca and M. P. Morales, *J. Appl. Phys.*, 2003, **94**, 3520; (b) R. Zboril, L. Machala, M. Mashlan, J. Tucek, R. Muller and O. Schneeweiss, *Phys. Stat. Solid.*, 2004, **1**, 3710.
- 6 E. V. Skorb, O. Baidukova, A. Goyal, A. Brotchie, D. V. Andreeva and H. Möhwald, *J. Mater. Chem.*, 2012, **22**, 13841.

